Low-temperature recombination luminescence of La-doped Ca_2SnO_4

U. Rogulis*, G. Krieke, A. Antuzevics, A. Fedotovs, Dz. Berzins, A.I. Popov, V. Pankratov

Institute of Solid State Physics, University of Latvia, 8 Kengaraga str., LV-1063, Riga, Latvia

*Corresponding author:

E-mail address: uldis.rogulis@cfi.lu.lv

Telephone number: +371-26774223

Abstract

Low-temperature ultraviolet-excited photoluminescence (PL) and recombination luminescence (RL) properties of La-doped Ca_2SnO_4 have been investigated by luminescence, electron paramagnetic resonance (EPR) and optically-detected magnetic resonance (ODMR) techniques. Two PL and RL bands at 340 nm and 450 nm have been observed. PL excitation spectra measurements with a synchrotron source showed a significant difference between the 450 nm and the 340 nm PL bands. The 450 nm band has a long-lasting hyperbolic decay, while the 350 nm band shows a fast decay. Assuming an excitonic nature of the 340 nm band, the band gap of the Ca_2SnO_4:La has been estimated to be approximately 5.5 eV. ODMR measurements suggest that the low-temperature RL band at 450 nm is caused by tunnelling recombination of electron trap and hole trap centres, and the recombination energy is transferred to Sn^{2+} luminescence centres.

Keywords: Calcium stannate, photoluminescence, afterglow, magnetic resonance, paramagnetic centres, recombination mechanism

Introduction

Rare-earth ion doped Ca_2SnO_4 has been widely investigated as a perspective phosphor in optics [1–7]. In this host, bright persistent luminescence can be achieved with most rare-earth elements, and the optimal dopant content typically is low [3,8,9]. Despite the extensive research performed on the host, information about the defect types in Ca_2SnO_4 is limited.

Recent electron paramagnetic resonance (EPR) spectroscopy studies of Ca_2SnO_4 have established that UV-generated paramagnetic centres play a significant role in the optical properties of the material [10,11]. In Al^{3+}-doped Ca_2SnO_4 the formation and decay of V-type and Sn^{3+} centres induce photochromism, i.e., reversible changes in the absorbance properties of the material [10]. If doped with rare-earth ions, Ca_2SnO_4 exhibits efficient and long-lasting persistent luminescence [3–7]. Recent investigations have demonstrated that different V- and F-type centres are generated in La^{3+}-doped Ca_2SnO_4 bright cyan persistent phosphor [11] in comparison to photochromic Ca_2SnO_4:Al^{3+} [10].

Although EPR is an excellent method for the analysis of paramagnetic defects, an unambiguous correlation between the defects and spectroscopic properties in persistent phosphors is challenging. Even if sample exposure to UV radiation generates paramagnetic centres, they are not necessarily involved in luminescence processes; therefore, additional experimental approaches need to be considered. One of the options is to establish an indirect correlation via combined analysis of EPR and luminescence spectroscopy measurements. For example, the temporal stability of paramagnetic centres can be compared with luminescence decay kinetics, or defect annealing kinetics – with a thermally stimulated luminescence (TSL) glow curve [11–13]. Such experiments provide valuable insights into the origin of persistent luminescence; however, the conclusions regarding the mechanisms are not always definitive.

Optically detected magnetic resonance (ODMR) methods in the form of photoluminescence-detected EPR (PL-EPR) as well as recombination-luminescence-detected EPR (RL-EPR) can be applied as an alternative approach for the studies of Ca_2SnO_4:La^{3+} and similar persistent phosphors. The most significant contribution of RL-EPR to the present research is that it allows a direct identification of the EPR centres participating in the recombination process. In the RL-EPR method microwave-induced changes of recombination luminescence intensity are measured showing the best resolution at high microwave frequencies and high magnetic fields.

In the present paper, the RL-EPR in the long-lasting afterglow as well as the PL-EPR of Ca_2SnO_4:La^{3+} have been investigated at low temperatures. Based on the identified paramagnetic electron and hole trap centres participating in the RL process, a mechanism for the 450 nm band is proposed.

Materials and methods

Microcrystalline Ca_2SnO_4 doped with 0.03 mol% La^{3+} was prepared using solid-state synthesis described in details in [11].

The phase composition of the samples was analysed with a Rigaku MiniFlex 600 X-ray diffractometer using a Cu Ka source operated at 40 kV and 15 mA.

Luminescence and luminescence decay were detected using an Andor Shamrock B-303i spectrometer coupled with an Andor Andor iSTAR DH734 CCD camera and photomultiplier tube (time resolution better than 20 ns). The measurements were performed using an Advanced Research Systems DE202 N cold finger type He cryostat, and a wavelength-tuneable pulsed solid-state laser Ekspla NT342/3UV was used as an excitation source.

Photoluminescence excitation spectra have been measured at the Superlumi endstation of the P66 beamline at PETRA III storage ring of the Photon Science Division of DESY synchrotron center (Hamburg, Germany). The technical parameters of the experimental setup can be found in [14].

Low-temperature (40-120 K) continuous-wave EPR spectra were measured with a Bruker ELEXSYS-II E500 CW-EPR spectrometer equipped with an Oxford Instruments liquid helium flow cryostat. The relevant spectra acquisition parameters were: 9.37 GHz microwave frequency; 2-20 mW microwave power; 0.4 mT magnetic field modulation amplitude and 100 kHz modulation frequency. Before EPR spectra measurements the sample was irradiated with a low-pressure Hg lamp at room temperature. Defect stability was investigated by step-wise sample annealing (10 min at selected temperature) in a custom-built furnace in air with an estimated temperature uncertainty of ± 10 °C. For EPR spectra simulations, EasySpin software [15] was used.

Optically detected magnetic resonance (ODMR) measurements were carried out using a custom-built spectrometer comprising an Oxford Instruments liquid helium cryostat with a superconducting magnet and optical access windows. The spectrometer has 62 GHz (V-band) and 97 GHz (W-band) microwave band options. All ODMR measurements were made at 1.5 K temperature and magnetic fields up to 3.8 T. The luminescence of the sample was detected with a Hamamatsu photomultiplier tube effectively

operating in the spectral range from 200 to 900 nm. A xenon lamp radiation filtered with a UV bandpass interference filter centred at 250 nm with 40 nm bandwidth was used for excitation of the sample photoluminescence in the PL-EPR and recombination luminescence in the RL-EPR measurements. Recombination luminescence detected EPR (RL-EPR) was measured in the afterglow luminescence after irradiating the sample for approximately 5 minutes at 1.5 K temperature. The RL-EPR signal was detected as the integral luminescence of the sample. The magnetic field dependent background was subtracted in all RL-EPR spectra. In the photoluminescence detected EPR (PL-EPR) measurements the sample was continuously irradiated with the aforementioned light source with the same UV filter and detected via a visible light bandpass filter transmitting from 310 to 780 nm. In PL-EPR detection microwave radiation was modulated with 3 Hz frequency and detected using the lock-in amplifier technique.

Results and discussion

X-ray diffraction

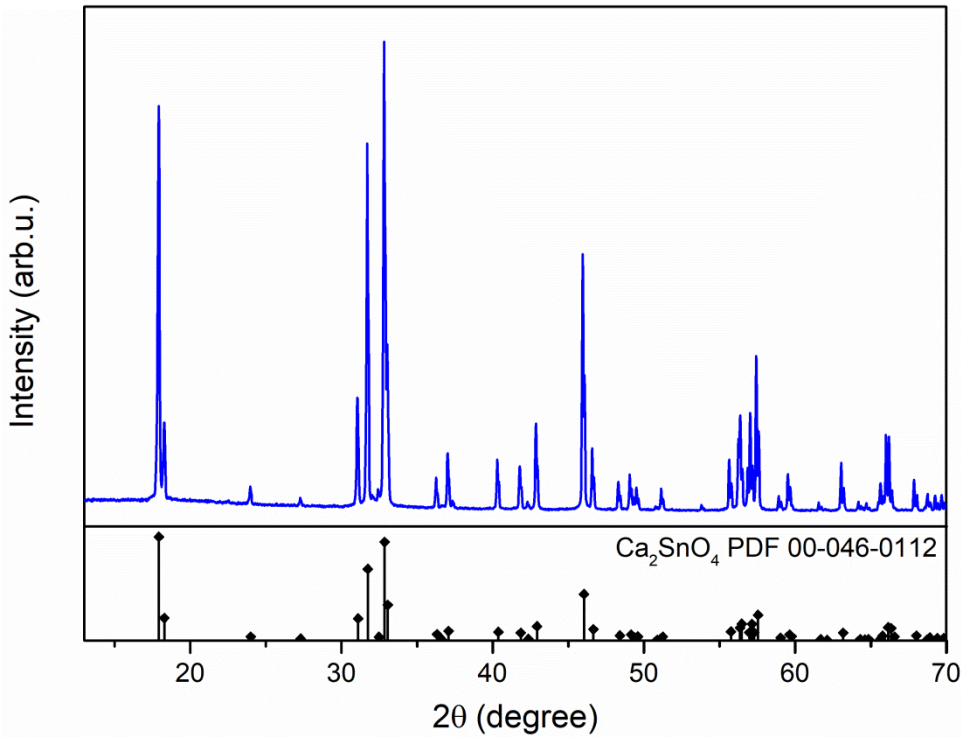

Figure 1. XRD pattern of the Ca_2SnO_4 sample doped with 0.03 mol% La^{3+}.

The phase composition of the prepared sample was analysed using X-ray diffraction analysis (see Fig. 1). The obtained XRD pattern coincides well with the standard diffraction lines of orthorhombic Ca_2SnO_4 (PDF 00-046-0112). No additional peaks could be detected indicating a complete reaction of precursors.

Luminescence

Short-wave UV excitation studies with a synchrotron source are valuable for elucidating luminescence excitation properties [16–18]. In the case of $Ca_2SnO_4:La^{3+}$ two distinct luminescence bands can be excited with a synchrotron source at low temperatures (as shown in the Fig. 2a).

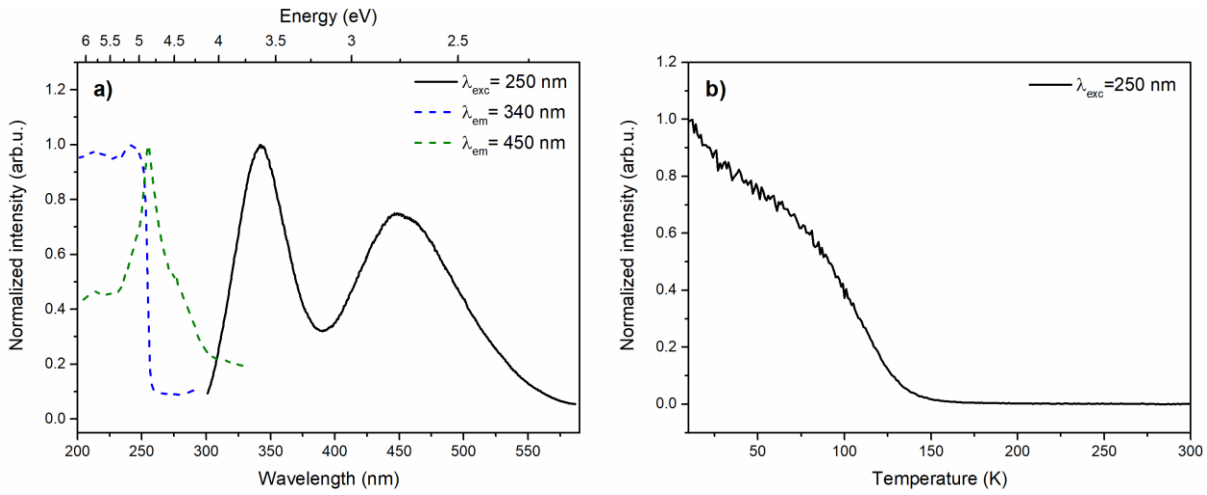

Figure 2. a) Photoluminescence excitation detecting 340 nm and 450 nm emission and photoluminescence (PL) spectrum excited with 250 nm detected at 10 K; b) temperature dependence of the 340 nm emission excited with 250 nm.

The band with the maximum centred at around 450 nm has been previously observed in stannate hosts [19–21] and can be attributed to the triplet to singlet state ($T_1 \rightarrow S_0$) transition of Sn^{2+}. The other band located at 340 nm can be detected only at low temperatures and exhibits rapid thermal quenching (see Fig. 2b).

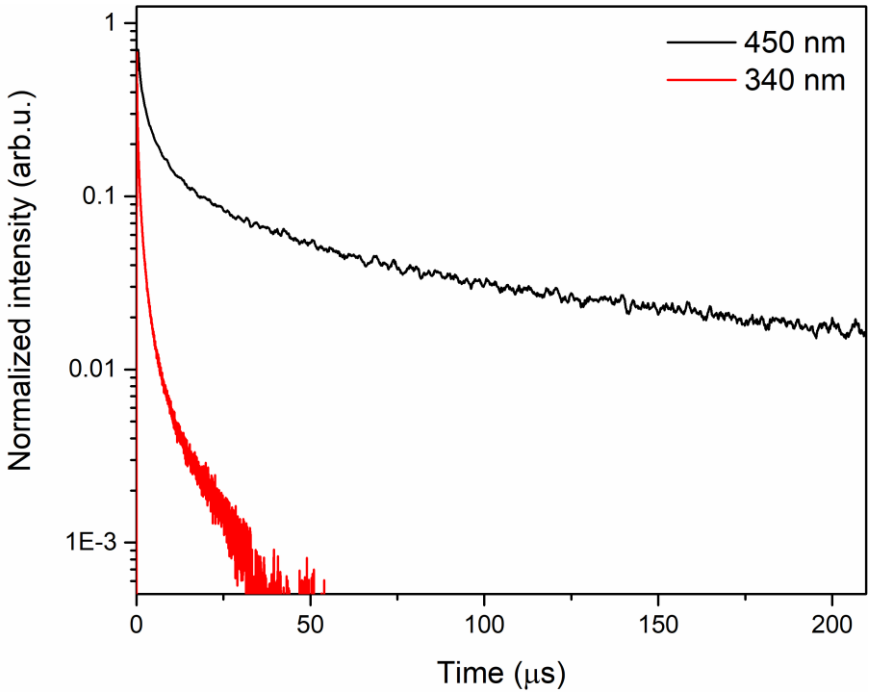

Figure 3. Decay kinetics of the 450 nm and 340 nm PL bands immediately after excitation.

The different decay times (see Fig. 3) confirm the dissimilar nature of the bands. The much longer 450 nm decay kinetics transforms into a prolonged hyperbolic RL decay (as will be discussed later, Fig. 4b).

The nature of the 340 nm band is different from the 450 nm band for the following reasons: (i) the two bands have different excitation spectra (Fig. 2a), (ii) the kinetics of the 340 nm band is fast (Fig. 3) and not hyperbolic, (iii) the 350 nm band has thermal quenching already up to 130 K (see Fig. 2b). Therefore, an excitonic nature for the 350 nm band could be proposed.

Assuming an excitonic nature of the 340 nm band with an excitation maximum E_{exc} at about 5.1 eV (see Figure 2a), we have used the phenomenological approach from Ref. [22] $E_g = 1.08\ E_{exc}$ to provide a bandgap estimation of 5.5 eV in Ca_2SnO_4:La. The excitation maximum E_{exc} 5.1 eV coincides rather well with the estimations given in [23,24].

Ca_2SnO_4: La^{3+} exhibits bright persistent luminescence related to Sn^{2+} emission at room temperature and 10 K. A comparison of PL and RL spectra detected at 10 K is shown in Fig. 4a)

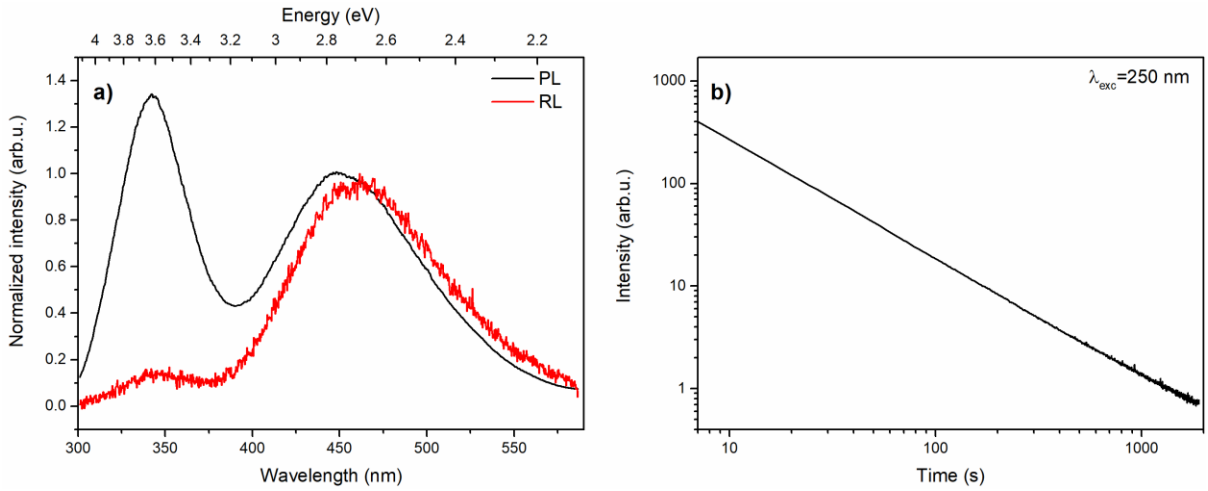

Figure 4. a) comparison of PL and RL spectra and b) RL decay curve excited with 250 nm detected at 10 K.

The 450 nm RL has a long-lasting hyperbolic decay kinetics after excitation (Fig. 4b), which is linear in double-logarithmic coordinates. Linear decay in double-logarithmic coordinates is characteristic for tunnelling recombination between spatially correlated electron and hole trap centre pairs [25,26].

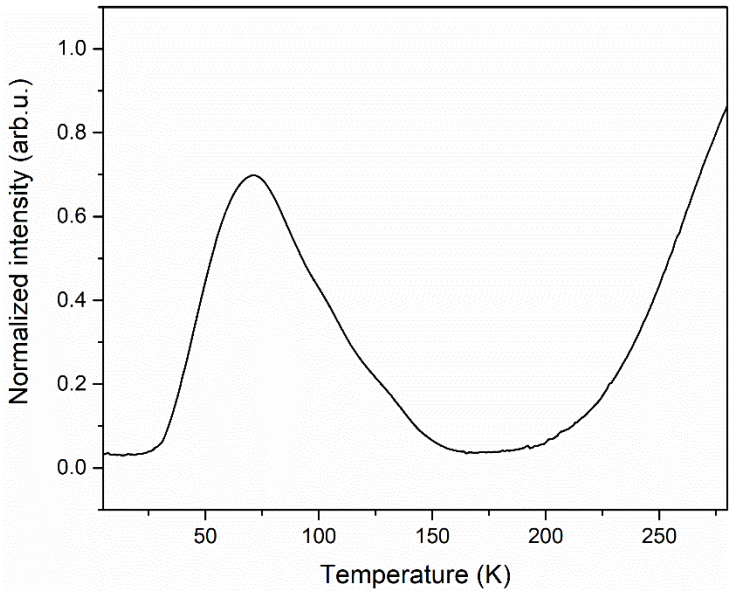

Figure 5. Thermostimulated luminescence in the 450 nm band at low temperatures after UV excitation at 10 K.

The samples exhibit a low-temperature peak with the maximum located at 70 K (Fig. 5). TSL is shown to start at about 30 K, which, in addition to the hyperbolic decay kinetics mentioned earlier, indicates that RL occurs as the tunnel recombination process.

EPR

Low-temperature EPR measurements were conducted to characterize paramagnetic defect formation and stability in Ca_2SnO_4. Spectra after the sample exposure to UV radiation and subsequent annealing at selected temperatures are demonstrated in Fig 6. Judging from the number, shape and relative intensities of the resonances, it is evident that several UV-induced paramagnetic centres contribute to the overall EPR spectrum. In contrast to the previous room-temperature EPR investigation of UV-induced defects in La-doped Ca_2SnO_4 [11], additional spectral features can be resolved in the spectra measured at 120 K. Most of the paramagnetic centres are annihilated after annealing at 100 °C, while several centres are stable up to 200 °C.

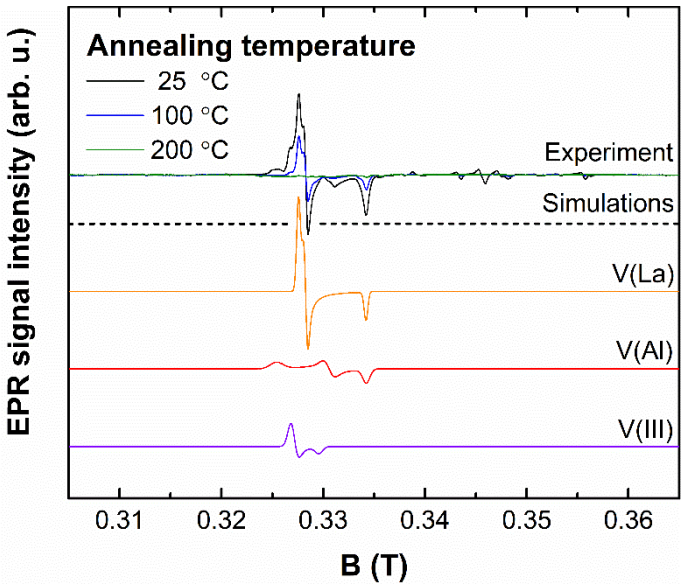

Figure 6. Experimental EPR spectra (120 K; 20 mW) after UV irradiation and subsequent annealing, and simulations of V-type centre signals contributing to the experimental EPR spectrum (120 K; 20 mW).

Analysis of the signals in 0.322-0.338 T range based on EPR spectra simulations is provided in Fig. 6. For the experimental microwave frequency of 9.37 GHz this field range corresponds to

$g > g_e$ (≈ 2.0023), which is characteristic to paramagnetic hole (V-type) centres [27–29]. The following spin-Hamiltonian (SH) was applied for the simulations:

$$H = g\mu_B BS \quad (1)$$

where g is the g-factor; μ_B – the Bohr magneton; B – external magnetic field; S – spin operator [30]. The individual paramagnetic centres were modelled as S = 1/2 systems with rhombic symmetry g-factors; the results of EPR spectra simulations are summarized in Table 1. Standard deviations of the g_i are given in the column Δg_i.

Table 1. A summary of SH parameters of paramagnetic centres in Ca_2SnO_4.

Centre	Material	g_1	g_2	g_3	Δg_i	Reference
V(La)		2.0430	2.0380	2.0020	0.0005	
V(Al)		2.0566	2.0244	2.0022	0.0005	
V(III)		2.0468	2.0458	2.0304	0.0020	
F(I)	$Ca_2SnO_4:La^{3+}$	1.9754	1.9369	1.9341	0.0010	Present study
F(II)		1.9170	1.8819	1.8811	0.0020	
F(III)		1.9511	1.9480	1.9480	0.0010	
F(IV)		1.9279	1.9261	1.9210	0.0020	
V-type	$Ca_2SnO_4:La^{3+}$	2.0425	2.0379	2.0024	0.0005	[11]
V-type	$Ca_2SnO_4:Al^{3+}$	2.0566	2.0244	2.0022	0.0005	[10]
F-type	$Ca_2SnO_4:La^{3+}$	1.9748	1.9366	1.9334	0.0005	[11]
Sn^{3+} I	$Ca_2SnO_4:Al^{3+}$		1.9940		0.0010	[10]
Sn^{3+} II	$Ca_2SnO_4:Al^{3+}$		1.9900		0.0050	[10]
Sn^{+}	$KCl:SnCl_2$	1.9149	1.7199	1.6788		[31]
Sn^{+}	$NaCl:Sn^{+}$	1.9000	1.7300	1.6300		[32]

The simulation results suggest that the observed spectrum is a superposition of signals of at least three V-type centres. For two of the centres the fitted parameter values are coincident with the results reported in the previous studies of Ca_2SnO_4 [10,11]. The centres have been interpreted as single trapped holes localized on oxygen ions (O^-) nearby either La^{3+} (designated as "V-type" in [11] or "V(La)" here) or Al^{3+} (designated as "V" in [10] or "V(Al)" here) substitutional impurities. The detection of such signals in the present investigation is expected as La^{3+} has been selected as the dopant ion, whereas Al^{3+} ions are commonly encountered trace impurities in oxide materials. In addition, the inclusion of the third

component was required to achieve a satisfactory fit between the experimental and simulation data. Based on the determined values of S and g, the centre could also be assigned to a single hole-type centre ("V(III)"), which is stabilized by a nearby impurity ion or cation vacancy.

Spectra acquisition at different temperatures and simulations with SH (1) were carried out for analysis of the spectral features in the 0.336-0.364 T range (Fig. 7). Signals in this spectral range are characterized by $g < g_e$, implying that they are associated with trapped electron (F-type) centres [27–29]. Dissimilar behaviour of EPR signal intensities on acquisition temperature for the different spectral features is observed, thus providing experimental evidence for the presence of several UV-generated F-type centres. Simulations were performed in a model of S = 1/2 with rhombic symmetry g; the results are summarized in Table 1. The fitted g values for the F(I) centre are coincident with the parameters reported in the room temperature investigations of $Ca_2SnO_4:La^{3+}$ [11]; however, the signals labelled as "F(II)-F(IV)" have not been previously detected.

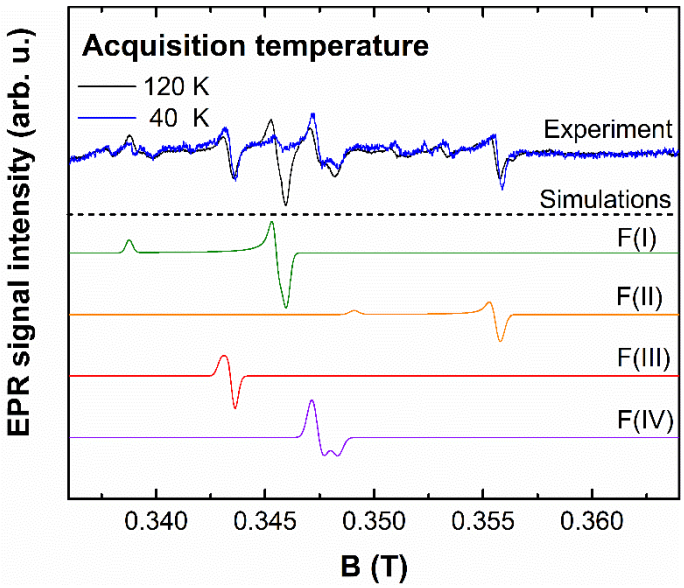

Figure 7. Simulations of F-type centre signals contributing to the experimental EPR spectra (40-120 K; 2 mW).

Several candidates should be considered as possible electron traps in $Ca_2SnO_4:La^{3+}$. Oxygen vacancies are common defects in oxide hosts, which form paramagnetic F^+ centres by trapping a single electron.

A variety of F^+ centres with significant deviations from the free electron value g_e have been reported in complex oxides, in which several anion sites are available in the crystal structure and antisite/impurity defects are present in the material [28,29]. However, considering the multi-valent nature of tin ions, UV-induced electron trapping on tin ions resulting in the formation of "EPR-active" Sn^{3+} [10,33–35] and Sn^+ [31,32] centres cannot be excluded in Ca_2SnO_4. Both oxidation states of tin are $S = 1/2$ systems and exhibit unique EPR spectra hyperfine structure due to electron spin interaction with spins of ^{117}Sn and ^{119}Sn nuclear isotopes. Attempts to detect the characteristic hyperfine structure in $Ca_2SnO_4:La^{3+}$ by prolonged spectrum acquisition in the 0-0.6 T range were unsuccessful; therefore, a qualitative analysis of the *g*-factor is provided. An isotropic g value of ≈ 1.99 has been reported for two Sn^{3+} centres in Al-doped Ca_2SnO_4 [10], whereas in the few EPR studies of Sn^+ centres in other hosts, highly anisotropic g values in $\approx$ 1.6-1.9 range have been determined [31,32]. Deviations from the data in Table 1 are significant, which suggests that the observed signals in this study are not related to paramagnetic tin centres. As the result, the most likely origin of the observed F-type signals in $Ca_2SnO_4:La^{3+}$ appears to be charged oxygen vacancy centres.

To prove the interrelation of paramagnetic centres with particular luminescence processes, additional experiments must be considered. For example, the involvement of the V(La) and F(I) centres in bright cyan blue persistent luminescence of $Ca_2SnO_4:La^{3+}$ at room temperature has been demonstrated by a correlated time-decay of the respective EPR signals and persistent luminescence kinetics [11]. The results of the present low-temperature EPR measurements reveal that additional paramagnetic centres partake in UV-induced processes of $Ca_2SnO_4:La^{3+}$. However, detailed analysis of the defect role in optical properties of the material by conventional EPR measurements alone is problematic due to defect stability at 120 K (signals do not decay with time) and signal saturation effects [30] at lower temperatures. Therefore, a more advanced methodology of optical detection of EPR signals is applied to explain the low-temperature luminescence characteristics of $Ca_2SnO_4:La^{3+}$.

RL-EPR

We investigated the RL-EPR of $Ca_2SnO_4:La^{3+}$ in the long-lasting afterglow as well as the PL-EPR in the 450 nm band at low temperatures. RL can be almost completely suppressed in magnetic field up to

3 T. By sweeping the magnetic field with the microwaves turned on, it is possible to restore the intensity of RL thus observing the RL-EPR resonances.

Experimental and simulation results of low-temperature RL-EPR investigations for two microwave frequency bands are shown in Fig. 8. Note that the registered signals are absorption profiles of RL, while EPR spectra (Fig. 6-7) are conventionally represented as the first derivative of microwave absorption. A satisfactory fit with the experimental spectra was achieved in a model with two S = 1/2 systems with: (1) g_1 = 2.04 ± 0.01; g_2 = 2.04 ± 0.01; g_3 = 2.00 ± 0.01 and (2) g = 1.95 ± 0.01. The determined parameter values are well-correlated with the EPR data of V(La) and F(III) paramagnetic centres (see Table 1).

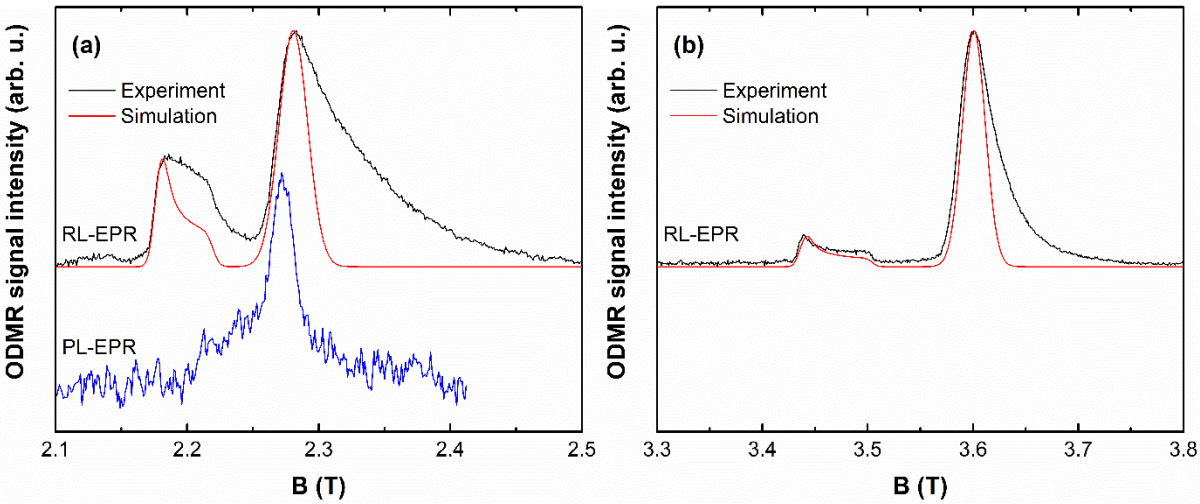

Figure 8. RL-EPR spectra measured at 62 GHz and (b) 97 GHz microwave frequencies and their calculation using the EPR parameters of the corresponding F-type (F (III)) and V-type (V (La)) centres. Blue line - PL-EPR spectrum measured at 62 GHz microwave frequency.

Measurements of the RL-EPR spectra with colour filters showed that the RL-EPR signals belong to the whole 450 nm RL band. The shape of the high field RL-EPR band is affected by the spin-lattice relaxation time T_1 [36] (see Fig. 8). Our estimations of the T_1 time is approximately 10 ± 5 seconds.

To observe PL-EPR during PL: (i) the magnetic field is swept, (ii) the change in PL intensity when switching on/off the microwave radiation is recorded. PL-EPR measurements clearly show (Fig. 8) only the resonance band at around g = 1.95, which corresponds to the similar F-type (F(III)) centre signal in

the RL-EPR spectra. This could be one of the evidences that RL makes up a competitive part of the PL process.

RL mechanism of the La-doped Ca_2SnO_4 at low temperatures

The main experimental features of the 450 nm RL band and the most probable model of the RL mechanism are discussed. The 450 band has hyperbolic decay kinetics and TSL starts at about 30 K above the RL-EPR measurement temperature of 1.5 K. A long-lasting hyperbolic afterglow decay is characteristic for the tunnelling recombination luminescence process. The 450 nm RL can be almost completely suppressed in magnetic field up to 3 T and restored after application of microwave radiation. RL-EPR shows resonances of both electron trap and hole trap centres. Several electron and hole trap centres are observed in the low-temperature EPR spectra of the UV irradiated sample. The *g*-factors of two of the paramagnetic centres are consistent with the RL-EPR signals. Therefore, we propose that the low-temperature RL band at 450 nm of the La-doped Ca_2SnO_4 after UV irradiation is caused by the tunnelling recombination of F-type (F(III)) and V-type (V(La)) centres.

The RL band originates either (i) directly by this tunnelling recombination of the F-V centres [37,38] or (ii) their recombination energy could be transferred to the Sn luminescence centre. So far, all previous references indicated that the 450 nm PL band could be originated by the Sn-luminescence; therefore, the mechanism (ii) seems to be preferable, as shown in the Fig. 9.

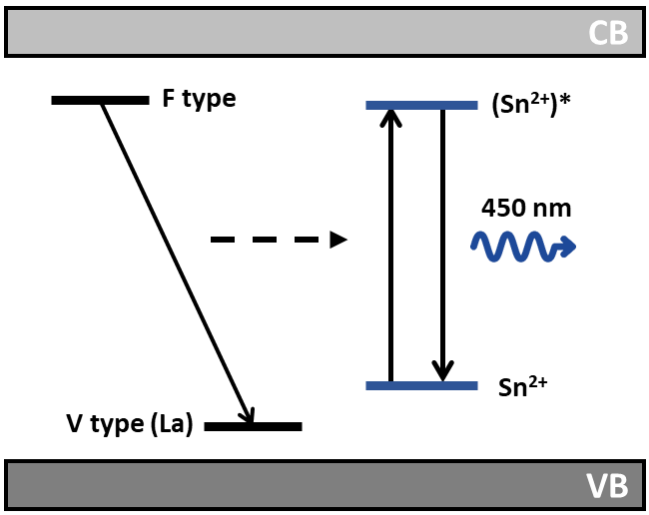

Figure 9. Low-temperature RL mechanism of Ca_2SnO_4:La. In PL, only the intra-centre luminescence of the Sn^{2+} is excited (right side).

Moreover, the band shape of the 450 nm RL is similar to the corresponding low-temperature PL band and it is only slightly shifted to longer wavelengths. The PL-EPR shows the resonance line of the same F-type centre as present in the RL-EPR spectra. The similarity of the band shape of the 450 nm RL and PL, and the PL decay kinetics suggest that the 450 nm PL band is interrelated with the RL.

Conclusions

Low-temperature PL and RL spectra of La-doped Ca_2SnO_4 after UV irradiation consist of 350 nm and 450 nm bands. The 350 nm band exhibits an exponential decay, is excited at shorter wavelengths near the band gap and has thermal quenching at low temperatures; therefore, it is likely of an excitonic nature. Assuming an excitonic nature of the 340 nm band, the band gap of the Ca_2SnO_4:La has been estimated to be approximately 5.5 eV. The 450 nm RL band has a long-lasting hyperbolic afterglow decay characteristic for tunnelling recombination. The shape of the RL band is similar to the corresponding low-temperature PL band; however, it is slightly shifted to longer wavelengths. The decay kinetics and the similarity of the RL and PL spectra suggest the 450 nm PL and RL have the same origin. The 450 nm RL band can be almost completely suppressed in magnetic field up to 3 T and restored after applying microwave radiation. RL-EPR spectra show resonances of both electron trap and hole trap centres. Several electron and hole trap centres are detected in the low-temperature EPR spectra in the UV irradiated sample. The *g*-factors of two of the paramagnetic centres are consistent with the RL-EPR signals. Therefore, we propose that the low-temperature 450 nm RL band of La-doped Ca_2SnO_4 after UV irradiation is caused by the tunnelling recombination of F-type electron trap and V-type hole trap centres. The RL band results from either direct tunnelling recombination of the F- and V-type centres or recombination energy transfer to Sn^{2+} luminescence centres and subsequent radiative relaxation.

Acknowledgements

This research is funded by the Latvian Council of Science, project "Novel persistent luminescent material – red light emitter", project No. LZP-2019/1-0443.

We acknowledge DESY (Hamburg, Germany), a member of the Helmholtz Association HGF, for the provision of experimental facilities. Parts of this research were carried out at PETRA III and we would like to thank Aleksei Kotlov for assistance in using the Superlumi setup. Beamtime was allocated for the proposal I-20210976 EC. The research leading to this result has been supported by the project CALIPSOplus under the Grant Agreement 730872 from the EU Framework Programme for Research and Innovation HORIZON 2020.

Institute of Solid State Physics, University of Latvia as the Centre of Excellence has received funding from the European Union's Horizon 2020 Framework Programme H2020-WIDESPREAD-01-2016-2017-TeamingPhase2 under grant agreement No. 739508, project CAMART².

References

[1] A. Stanulis, A. Katelnikovas, D. Enseling, D. Dutczak, S. Šakirzanovas, M. Van Bael, A. Hardy, A. Kareiva, T. Jüstel, Luminescence properties of Sm^{3+}-doped alkaline earth ortho-stannates, Opt. Mater. (Amst). 36 (2014) 1146–1152. https://doi.org/10.1016/j.optmat.2014.02.018.

[2] A. Stanulis, A. Katelnikovas, M. Van Bael, A. Hardy, A. Kareiva, T. Justel, Photoluminescence of Pr^{3+}-doped calcium and strontium stannates, J. Lumin. 172 (2016) 323–330. https://doi.org/10.1016/j.jlumin.2015.11.021.

[3] T. Ishigaki, A. Torisaka, K. Nomizu, P. Madhusudan, K. Uematsu, K. Toda, M. Sato, Long phosphorescent Ca_2SnO_4 with minuscule rare earth dopant concentration, Dalt. Trans. 42 (2013) 4781. https://doi.org/10.1039/c3dt33079f.

[4] B. Zhang, M. Shi, D. Zhang, Y. Guo, C. Chang, W.J. Song, The comparison: photoluminescence and afterglow behavior in $CaSnO_3$:Dy^{3+} and Ca_2SnO_4:Dy^{3+} phosphors, J. Mater. Sci. Mater. Electron. 28 (2017) 11624–11630. https://doi.org/10.1007/s10854-017-6964-9.

[5] J. Ma, Y. Chen, X. Wang, S. Cao, Q. Chen, Luminescent performance of Ca_2SnO_4:Tb^{3+} phosphors with Li^+ co-doping, Opt. Mater. (Amst). 85 (2018) 86–90. https://doi.org/10.1016/j.optmat.2018.08.036.

[6] Y. Chen, J. Ma, Q. Chen, S. Cao, X. Wang, Preparation of Ca_2SnO_4:Tb^{3+}, R^{3+} phosphors (R^{3+} = B^{3+}, Al^{3+} or Ga^{3+}) and the dependence of their luminescence on R^{3+} cations, Opt. Mater. (Amst). 91 (2019) 408–412. https://doi.org/10.1016/j.optmat.2019.03.056.

[7] D. Zhang, M. Shi, Y. Sun, Y. Guo, C. Chang, Long afterglow property of Er^{3+} doped Ca_2SnO_4 phosphor, J. Alloys Compd. 667 (2016) 235–239. https://doi.org/10.1016/j.jallcom.2016.01.081.

[8] B. Lei, H. Zhang, W. Mai, S. Yue, Y. Liu, S. Man, Luminescent properties of orange-emitting long-lasting phosphorescence phosphor Ca_2SnO_4:Sm^{3+}, Solid State Sci. 13 (2011) 525–528. https://doi.org/10.1016/j.solidstatesciences.2010.12.019.

[9] G. Krieke, A. Antuzevics, K. Smits, D. Millers, Enhancement of persistent luminescence in

Ca_2SnO_4: Sm^{3+}, Opt. Mater. (Amst). 113 (2021) 110842. https://doi.org/10.1016/j.optmat.2021.110842.

[10] G. Krieke, A. Antuzevics, B. Berzina, Defect formation in photochromic Ca_2SnO_4: Al^{3+}, Mater. Today Commun. 28 (2021) 102592. https://doi.org/10.1016/j.mtcomm.2021.102592.

[11] A. Antuzevics, G. Krieke, G. Doke, B. Berzina, The origin of bright cyan persistent luminescence in Ca_2SnO_4:La^{3+}, Materialia. 21 (2022) 101374. https://doi.org/10.1016/j.mtla.2022.101374.

[12] J. Ueda, A. Hashimoto, S. Tanabe, Orange Persistent Luminescence and Photodarkening Related to Paramagnetic Defects of Nondoped CaO-Ga_2O_3-GeO_2 Glass, J. Phys. Chem. C. 123 (2019) 29946–29953. https://doi.org/10.1021/acs.jpcc.9b07638.

[13] G. Doke, A. Antuzevics, G. Krieke, A. Kalnina, M. Springis, A. Sarakovskis, UV and X-ray excited red persistent luminescence in Mn^{2+} doped $MgGeO_3$ material synthesized in air and reducing atmosphere, J. Lumin. 234 (2021) 117995. https://doi.org/10.1016/j.jlumin.2021.117995.

[14] V. Pankratov, A. Kotlov, Luminescence spectroscopy under synchrotron radiation: From SUPERLUMI to FINESTLUMI, Nucl. Instruments Methods Phys. Res. Sect. B Beam Interact. with Mater. Atoms. 474 (2020) 35–40. https://doi.org/10.1016/j.nimb.2020.04.015.

[15] S. Stoll, A. Schweiger, EasySpin, a comprehensive software package for spectral simulation and analysis in EPR, J. Magn. Reson. 178 (2006) 42–55.

[16] V. Nagirnyi, L. Jönsson, M. Kirm, A. Kotlov, A. Lushchik, I. Martinson, A. Watterich, B.I. Zadneprovski, Luminescence study of pure and Fe- or Mo-doped ZnWO4 crystals, Radiat. Meas. 38 (2004) 519–522. https://doi.org/10.1016/j.radmeas.2004.01.024.

[17] E. Feldbach, E. Tõldsepp, M. Kirm, A. Lushchik, K. Mizohata, J. Räisänen, Radiation resistance diagnostics of wide-gap optical materials, Opt. Mater. (Amst). 55 (2016) 164–167. https://doi.org/10.1016/j.optmat.2016.03.008.

[18] V.N. Makhov, C. Lushchik, A. Lushchik, M. Kirm, Z.F. Wang, W.P. Zhang, M. Yin, J.T. Zhao, Multiplication of electronic excitations in nanophosphors Lu_2O_3:Eu^{3+} and Lu_2O_3:Tb^{3+}, J. Lumin. 129 (2009) 1711–1714. https://doi.org/10.1016/j.jlumin.2008.12.028.

[19] Y. Suzuki, M. Kakihana, Parallel solution-based synthesis approach for search of lanthanoid-activated Ca_2SnO_4 phosphor materials, J. Am. Ceram. Soc. 92 (2009) 168–171. https://doi.org/10.1111/j.1551-2916.2008.02706.x.

[20] C. Zheng, Q. Liu, Luminescent properties of a new cyan long afterglow phosphor $CaSnO_3$:Lu^{3+}, RSC Adv. 9 (2019) 33596–33601. https://doi.org/10.1039/c9ra07107e.

[21] M. Shi, H. Zhao, J. Zou, B. Yang, Y. Li, Z. Wang, C. Chang, W. Li, Preparation and characterization of a new long afterglow phosphor $CaSnO_3$: Yb^{3+}, J. Mater. Sci. Mater. Electron. 28 (2017) 10067–10072. https://doi.org/10.1007/s10854-017-6767-z.

[22] P. Dorenbos, Charge transfer bands in optical materials and related defect level location, Opt. Mater. (Amst). 69 (2017) 8–22. https://doi.org/10.1016/j.optmat.2017.03.061.

[23] P. Dorenbos, The Electronic Structure of Lanthanide Impurities in TiO_2, ZnO, SnO_2, and Related Compounds, ECS J. Solid State Sci. Technol. 3 (2014) R19–R24. https://doi.org/10.1149/2.005403jss.

[24] S.K. Gupta, K. Sudarshan, B. Modak, A.K. Yadav, P. Modak, S.N. Jha, D. Bhattacharyya, Achieving Bright Blue and Red Luminescence in Ca_2SnO_4 through Defect and Doping Manipulation, J. Phys. Chem. C. 124 (2020) 16090–16101. https://doi.org/10.1021/acs.jpcc.0c03180.

[25] C.J. Delbecq, D.L. Dexter, P.H. Yuster, Tunneling-recombination luminescence between Ag^0 and Ag^{2+} in KCl:AgCl, Phys. Rev. B. 17 (1978) 4765–4774. https://doi.org/10.1103/PhysRevB.17.4765.

[26] T. Tashiro, S. Takeuchi, M. Saidoh, N. Itoh, Luminescence induced by tunnelling recombination between neutral silver atoms and V_K centres in alkali halides, Phys. Status Solidi. 92 (1979) 611–618. https://doi.org/10.1002/pssb.2220920234.

[27] A.E. Hughes, B. Henderson, Color Centers in Simple Oxides, in: Point Defects in Solids, 1972: pp. 381–490. https://doi.org/10.1007/978-1-4684-2970-1_7.

[28] M. Nikl, V. V. Laguta, A. Vedda, Complex oxide scintillators: Material defects and scintillation performance, Phys. Status Solidi Basic Res. 245 (2008) 1701–1722. https://doi.org/10.1002/pssb.200844039.

[29] V. V. Laguta, M. Nikl, A. Vedda, E. Mihokova, J. Rosa, K. Blazek, Hole and electron traps in the $YAlO_3$ single crystal scintillator, Phys. Rev. B - Condens. Matter Mater. Phys. 80 (2009) 1–10. https://doi.org/10.1103/PhysRevB.80.045114.

[30] J.A. Weil, J.R. Bolton, Electron Paramagnetic Resonance, Wiley, 2007.

[31] C.J. Delbecq, R. Hartford, D. Schoemaker, P.H. Yuster, Sn^+ Centers in KCl:$SnCl_2$, Phys. Status Solidi. 71 (1975) K81–K85. https://doi.org/10.1002/pssb.2220710160.

[32] P.G. Baranov, V.A. Khramtsov, EPR Study of Impurity Colour Centres in P-State in Alkali Halides, Phys. Status Solidi. 101 (1980) 153–161. https://doi.org/10.1002/pssb.2221010116.

[33] I. Jaek, E. Realo, V. Seman, L. Mürk, NGR, EPR, and Optical Characteristics of Sn Centres in CaS, Phys. Status Solidi. 61 (1974) 745–755. https://doi.org/10.1002/pssb.2220610243.

[34] N. Yamashita, S. Asano, ESR of 2S12/-state centres in CaS:Sn^{3+}, CaSe:Sn^{3+} and CaSe:Pb^{3+}, J. Phys. C Solid State Phys. 9 (1976). https://doi.org/10.1088/0022-3719/9/3/003.

[35] Z. Egemberdiev, K. Realo, S. Zazubovich, Haldre, T. Lehto, S. Reifman, V. Seeman, Polarized luminescence and EPR study of Sn^{3+} centres in KCl:$SnCl_2$ crystals, Phys. Status Solidi. 96 (1979) 867–875. https://doi.org/10.1002/pssb.2220960243.

[36] N.G. Romanov, Y.P. Veshchunov, V.A. Vetrov, P.G. Baranov, Application of tunneling recombination afterglow for EPR optical detection of recombining centres in ionic crystals, Phys. Status Solidi. 107 (1981) K119–K124. https://doi.org/10.1002/pssb.2221070255.

[37] U. Rogulis, J.M. Spaeth, I. Tale, M. Nikl, N. Ichinose, K. Shimamura, Magnetooptical studies of defects and recombination luminescence in $LiBaF_3$, Radiat. Meas. 38 (2004) 663–666. https://doi.org/10.1016/j.radmeas.2004.03.013.

[38] M. Secu, S. Schweizer, U. Rogulis, J.M. Spaeth, Radiation-induced defects and their recombination processes in the x-ray storage phosphor $BaBr_2$:Eu^{2+}, J. Phys. Condens. Matter. 15 (2003) 2061–2070. https://doi.org/10.1088/0953-8984/15/12/323.